

## Article

# Energy Dissipation Enhancement of Thin-Walled 6063 T5 Aluminium Tubes by Combining a Triggering Mechanism and Heat Treatment

Jorge Jiménez-Armendáriz <sup>1,†</sup>, Moises Jimenez-Martinez <sup>1,\*,†</sup>, Julio Varela-Soriano <sup>1,†</sup>, Alfredo Santana Diaz <sup>2</sup>   
and Rogelio Perez Santiago <sup>3</sup> 

<sup>1</sup> Tecnológico de Monterrey, Campus Puebla, Escuela de Ingeniería y Ciencias, Puebla 72453, Mexico

<sup>2</sup> Tecnológico de Monterrey, Campus Toluca, Escuela de Ingeniería y Ciencias, Toluca de Lerdo 50110, Mexico

<sup>3</sup> Tecnológico de Monterrey, Campus Querétaro, Escuela de Ingeniería y Ciencias, Santiago de Querétaro 76130, Mexico

\* Correspondence: moisesjimenezmartinez@gmail.com or mjimenezm@tec.mx

† These authors contributed equally to this work.

**Abstract:** It is necessary to reduce the weight of components while maintaining or improving their mechanical properties to withstand dynamic loads in lightweight structures. In this study, heat treatment and a trigger mechanism were implemented for a thin-walled tube of aluminium to increase energy absorption while reducing the peak crushing force. Different geometries and locations were proposed to trigger deformation in a controlled manner, in combination with heat treatments. Experimental designs for each energy absorption mechanism were performed, and designs were tested by quasi-static crushing. Data obtained from experiments were used to calculate energy absorption indicators that were used to compare designs with components without mechanism to analyse performance. By comparing proposed designs with tubes without modification, the best combination of design variables for each trigger mechanism were identified. It was determined that 160 mm from the upper side, 250 mm<sup>2</sup> area and a rectangular trigger shape reduced peak crushing force by 22.03% and increased energy absorption by 37.76%. For heat treatment, the optimal combination was heating in a furnace at 175 °C for 1 h and cooling in water at 70 °C during 10 min while only soaking half of its length. This combination reduced peak crushing force by 19.02% and increased energy absorption 15.08%. When these mechanisms were combined on a single tube, peak crushing force was reduced by 21.63%, and energy absorption increased by 42.53%.

**Keywords:** lightweight structures; aluminium; energy absorption; heat treatments; crushing



**Citation:** Jiménez-Armendáriz, J.; Jimenez-Martinez, M.; Varela-Soriano, J.; Santana-Diaz, A. and Perez-Santiago, R. Energy Dissipation Enhancement of Thin-Walled 6063 T5 Aluminium Tubes by Combining a Triggering Mechanism and Heat Treatment. *Metals* **2023**, *13*, 922. <https://doi.org/10.3390/met13050922>

Academic Editor: John D. Clayton

Received: 20 April 2023

Revised: 6 May 2023

Accepted: 7 May 2023

Published: 9 May 2023



**Copyright:** © 2023 by the authors. Licensee MDPI, Basel, Switzerland. This article is an open access article distributed under the terms and conditions of the Creative Commons Attribution (CC BY) license (<https://creativecommons.org/licenses/by/4.0/>).

## 1. Introduction

In the automotive industry, manufacturers and suppliers have an increasing interest in designing vehicles and their components to provide security to passengers without increasing the mass of the structure. During the development of an impact, are developed three main phenomena, the impact of the vehicle versus another vehicle or an object, the impact of the driver or occupants with vehicle interiors and the impact of the organs with internal parts of the body. Because of this, after the first energy peak developed by the absorber, it is important to control the way energy is absorbed to attenuate the generation of peaks during the controlled deformation process [1,2]. Crashworthiness design criteria have even greater importance for structures that are designed to withstand impact conditions. Two indicators are used to determine the energy absorption capability of a structure: the amount of energy dissipated by deformation and the peak crushing force registered during deformation. The peak crushing force is related to deceleration during impact, and the energy absorption is determined by measuring the value of the crushing force as the structure deforms [3–5].

For electrical vehicles, where autonomy is a key factor of performance, vehicle manufacturers must reduce structural mass by optimising design geometry or using lighter materials. Reducing the mass increases the battery charge duration because less mass means less power is required to keep the vehicle in movement. Aluminium is broadly used as an alternative to steel in vehicle chassis for designing lighter automotive structures [6,7]. Even though aluminium has only half of the yield strength of steel, it has only one-third of its density. The specific strength, which is the ratio of yield strength to density, for aluminium is 40% greater than that of steel. This means that using aluminium instead of steel could reduce the mass by 40%, but it is still necessary to consider the reduction in strength.

For vehicles, mechanical impact is the critical design consideration, with the most common load case being frontal impact. The component involved in this load case is the frontal rail, specifically the crash box (Figure 1). The purpose of the crash box is to dissipate kinetic energy of the impact into mechanical deformation, preventing deformed structures from reaching the passenger compartment and reducing deceleration during deformation [8–10]. The principle of kinetic energy dissipation by deformation is called energy absorption, and components that withstand impact forces are designed with materials and geometries to increase the maximum amount of energy dissipated by plastic deformation. A crash box is formed from a metal sheet into a shape with constant cross section, such as a thin-walled tube. Many energy absorption studies have focused on the behaviour of thin-walled structures during impact, and findings on thin-walled structures can be applied to crash boxes and components with similar shapes [11,12].

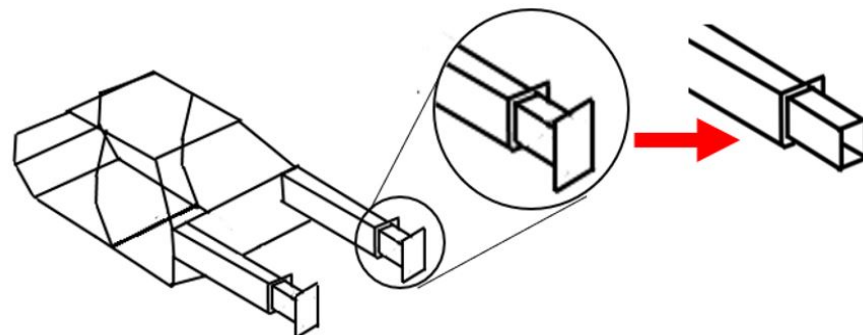


**Figure 1.** Typical crash box structure and similarity with a thin wall tube, in the right is shown a zoom view without frontal plate.

Researchers studying thin-walled structures seek to develop geometries that have great energy absorption but without increasing the peak crushing force and reducing the component mass [13,14]. In general, reducing the peak crushing force and optimising energy absorption cannot be accomplished with a single solution because a design that optimises energy absorption could increase peak crushing, and a design that reduces peak crushing force could decrease energy absorption [15,16].

Plastic deformation is preferred over mechanical fracture in terms of energy absorption because if the component has not yet broken, it can continue deforming, and thus, it dissipates more energy. The crushing behaviour of thin-walled structures depends on their length, thickness, cross-sectional shape, material, and load case. By controlling these parameters, crushing behaviour can be managed to prioritise progressive buckling over fracture or global bending and increase the amount of energy absorbed [17].

On thin-walled structures under axial impact loading, the most common deformation mechanism is progressive axial buckling, which is the subsequent deformation of plastic hinges until the entire length of the structure is deformed. Depending on whether loaves fold inwards or outwards, folding can be symmetric or asymmetric. Symmetric folding leads to the formation of new folds. If the number of asymmetric folds increases, then it also increases the probability of a transition from progressive buckling to Euler buckling.

An excess of asymmetric plastic hinges leads to fracture of the tube. The subsequent formation of one plastic hinge after another is called progressive buckling, and the formation of a single plastic hinge and deviation of the tube axis is called global buckling [18].

Progressive buckling is not the natural collapse mechanism of deformation in all thin-walled structures during impact or quasi-static crushing, and progressive buckling can be induced by reducing strength in specific sections of thin walls of structures. Holes with specific shapes drilled or machined in walls are called triggers. This method is called the triggering mechanism [19–21]. Imperfections of the structure of a wall can also reduce the peak crushing force by reducing the mechanical strength. Estrada et al. [22] evaluated the mechanical effects of stress concentrators using finite element analysis.

The position as well as the geometry of a deformation initiator is important at the beginning of the collapse of a component. The result may be that the component fractures, decreasing its controlled absorption capacity. To improve its properties, zoned heat treatments can be used, which help to control the first peak of deceleration generated by the inertia between components [23]. Then, it is important to maintain a constant level of absorbed energy, which depends on the folds generated before a fracture develops. It has been made possible to improve the energy absorption capacity not only by reducing the peak crushing force but also by improving the absorption capacity throughout the deformation of the component. Heat treatment design variables were amount of time in the furnace, cooling rate using water at different temperatures, and choice of cooling method, i.e., dipping the entire tube or only half of the tube.

Another method to control the buckling behaviour of thin-walled structures and energy absorption is heat treatment. Heat treatment is used to control the mechanical properties of metals. In the case of energy absorption, heat treatment can produce variable strength along the length of the structure, which can lead to the formation of plastic folds in a specific location of the structure, controlling buckling behaviour. Additionally, increasing or decreasing structural strength or ductility can be used to control energy absorption and peak crushing force [24]. For aluminium, due to its alloying materials, the heat treatment can involve artificial ageing, which consists of heating the tube in a furnace for a specific time, allowing oversaturated phases formed during manufacturing to precipitate. These precipitated phases increase mechanical strength by blocking dislocations [25].

This study proposed a thin-walled design that combined a trigger mechanism and heat treatment. Experimental designs from each energy absorption enhancement mechanism were performed separately, and then the best combination was applied to the same tube. The goal was to reduce the peak crushing force and increase the absorbed energy in comparison to an untreated tube. Finite element analysis was performed in the *RADIOSS* simulating experimental test and dynamic crushing test. Analyses of correlations and fitting experimental data were performed. The experimental design for determining the optimal trigger pattern was performed in three phases. In the first phase, the design variables were trigger geometry, size and distance from the upper side. The relationship among these three variables was analysed. In the second phase, the area of the trigger and distance from the upper side were kept constant, and only the shape was varied; the best shape was determined. For the third phase, the shape from the previous phase and the distance from the upper side were kept constant, and the size was varied. Finally, it can provide the best combination of distance from the upper side, size and trigger shape for energy absorption and crushing force.

The interest of developing a hybrid system is to control two main processes during impact absorption. The first peak of force is where the maximum deceleration occurs, and which contains the greatest stabilisation of energy throughout the collapse, without breaking the component. Because of this, the aim is to control the area and shape of the beginning of deformation through imperfection, but later to stabilise the energy through heat treatment. To dissipate a control de deformation, an evaluation was developed to improve the precipitation phase after the pre-aging treatment. The aluminium can be quenched and precipitation is made at 205 °C for one hour to achieve a T5; by changing

the process to a temperature of 175 °C for 8 h, a T6 is obtained. To develop a system with high tenacity, aging is carried out at 175 °C for furnace times from 1 to 72 h. Based on these parameters, an evaluation was developed to improve the precipitation phase after the pre-aging treatment. A hybrid system was developed by increasing the precipitation of magnesium and silicon, generating greater diffusion, which can be used to absorb impact energy without shearing the component. The originality of this study is that it proposes a crashworthiness enhancement method. This new method combines a trigger mechanism and heat treatment to reduce the peak crushing force. As a consequence, the energy absorption is improved. It is also important to mention that this method was validated using the numerical and experimental simulations, which are then evaluated.

## 2. Energy Absorption Evaluation

Regarding crashworthiness, it is important to determine which designs and materials have better capacities to dissipate energy as plastic deformation. To determine how much energy is dissipated as deformation, it is necessary to measure the crushing force and the deformation of the material during crushing. The area under the curve of the load (crushing force) vs. deformation curve is equal to the energy dissipated as deformation, as shown in Figure 2. According to Equation (1):

$$E = \int_0^{\delta} F(\delta) \cdot d\delta \quad (1)$$

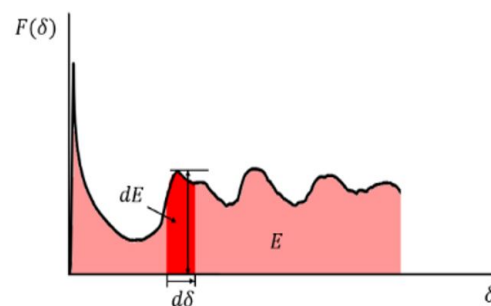


**Figure 2.** Load vs. displacement curve.

Energy absorption indicators can be obtained from the load displacement curve and are used to determine the performance of the proposed design and determine whether it fits the design requirements. In this study, it was sought for a design that reduced crushing force more than energy absorption loss due to reduced strength [26].

Specific Energy Absorption (*SEA*) is the energy absorbed by a mass [27]. This parameter is used to choose between two designs and to select the one that absorbs more energy (*E*) in less mass (*m*); it is expressed by:

$$SEA = \frac{E}{m} \quad (2)$$

Contraction efficiency (*S<sub>E</sub>*) is the ratio of length reduction (*δ*) after collapse and the original length of the material (*L<sub>0</sub>*) [28], defined in Equation (3):

$$S_E = \frac{\delta}{L_0} \quad (3)$$

The mean crushing force (*MCF*) is the ratio of energy absorbed to length reduction [29], and this parameter is useful when the length is reduced, as expressed by Equation (4):

$$MCF = \frac{E}{\delta} \quad (4)$$

The peak crushing force is the maximum crushing force in the load vs. displacement curve. This parameter approximates the average force of the material during collapse. When a vehicle crashes into another vehicle or an obstacle, the chassis deforms due to kinetic energy and the sudden reduction in the speed of the vehicle. If stiffness is reduced, the peak crushing force is also be reduced. For OEMs (Original Equipment Manufacturers), reduction of the peak crushing force is important because it also reduces the peak acceleration. The crushing force efficiency ( $CFE$ ) is the ratio of the mean crushing force ( $MCF$ ) and peak crushing force ( $PCF$ ); see Equation (5):

$$CFE = \frac{MCF}{PCF} \quad (5)$$

This indicator is used to determine the size of the peak crushing force in comparison to the mean crushing force. If the peak crushing force is close to the mean crushing force, then the collapse is more stable. A larger  $CFE$  means a more stable collapse, and a smaller value means a larger reduction in peak acceleration [30].

Energy efficiency ( $e_E$ ) is directly proportional to absorbed energy and inversely proportional to the product of peak crushing force and initial length, which means that to obtain the greatest energy efficiency, a combination of small peak crushing force and initial length but with great energy absorption is necessary [31].

$$e_E = \frac{E}{PCF \cdot L_0} = \frac{MCF \times \delta}{PCF \times L_0} = CFE \times S_E \quad (6)$$

This parameter is used to choose among designs because the design with the highest energy efficiency meets the requirements of OEM or market regulations that are small peak crushing force and large energy absorption. The work efficiency ( $W_{eff}$ ) is the product of the  $SEA$  and contraction efficiency ( $S_E$ ), expressed as:

$$W_{eff} = SEA \times S_E \quad (7)$$

This parameter describes the combination of low mass and the ability to fit spatial requirements. The dynamic application factor ( $FDA$ ) is the ratio of energy absorption to energy absorption for a quasi-static load and given displacement. Its formula is:

$$FDA = \frac{E_d}{E_{qs}} \quad (8)$$

where  $E_d$  is the dynamic energy absorbed and  $E_{qs}$  is the quasi-static energy absorbed. This factor helps to determine the strain hardening effect on the material, and a material with greater strain rate hardening absorbs more energy for a dynamic load than a quasi-static load. These indicators are used to determine whether an energy absorption enhancement mechanism applied to a thin-walled tube increases its crashworthiness characteristics [32].

Thin-walled tubes absorb energy in the form of deformation, and almost all the deformation in a buckling collapse is plastic deformation. Conventional linear elastic models do not cover all the phenomena that are needed to determine the values of stress and deformation. The Johnson Cook model is one of the models used in finite element analysis to determine the values of stresses under a given deformation [33]. This is expressed by:

$$\bar{\sigma} = \left[ \sigma_0 + Q_R(1 - \exp(-C_R \bar{\epsilon})) \right] [1 + \dot{\epsilon}^*]^{Cv^*} \left[ 1 - T^{*M} \right] \quad (9)$$

where  $\bar{\sigma}$  is the effective stress,  $\sigma_0$  is the yield stress,  $Q_R$  is the hardening constant,  $\bar{\epsilon}$  is the unitary effective plastic deformation,  $\dot{\epsilon}^*$  is the dimensionless strain,  $Cv^*$  quantifies the strain rate sensitivity of the material,  $M$  defines thermal softening and  $T^*$  is the homologous temperature.

In this study, finite element simulations are performed on Altair Hypermesh using the nonlinear solver RADIOSS. The material card used for nonlinear elasto-plastic materials is *M2 PLAS JOHNS ZERIL* [34]. This card calculates stress and strain according to:

$$\sigma = (A + B\varepsilon^n)(1 + C \ln \dot{\varepsilon}^*) (1 - T^{*m}) \quad (10)$$

For quasi-static conditions, heat transfers are small in comparison with other energy dissipations, and  $(1 - T^{*m})$  is equal to 1, which leaves the equation as:

$$\sigma = (A + B\varepsilon^n)(1 + C \ln \dot{\varepsilon}^*) \quad (11)$$

where  $A$  is the yield stress,  $C$  is the strain rate (rate of deformation during collapse) and  $B$  and  $n$  are calculated from two points on the strain stress curve

### 3. Materials and Methods

#### 3.1. Mechanical Characterisation

Quasi-static crushing tests were performed on an *INSTRON-Norwood, Massachusetts, USA* universal testing machine. This equipment had the capacity to perform both tensile and compressive tests, quasi-static crushing, and tensile tests. The material was a tube of aluminium 6063 T5 alloy with square cross section, and each specimen was 200 mm in length, 1.5 mm in thickness and 2 mm in side length. Each sample was tested by quasi-statically crushing the tube on an *INSTRON* universal testing machine at a rate of 70 mm/min. The values of force and deformation during crushing were automatically recorded by the machine and used to determine energy absorption indicators, which were used to determine the best performance in each experimental design.

To analyse the characteristics of the heat treatments, a series of heat treatments were carried out to optimise the process. Heat treatments were performed using two electrical furnaces with a 1100 °C heat limit and ceramic internal layer. The selected cooling method was water, which was heated to determine the temperature using resistance and monitored with thermocouples. Quasi-static properties are shown in Figure 3 and summarised in Table 1.

**Table 1.** Mechanical properties of heat-treated aluminium.

Furnace Time (h)	Cooler Temperature (°C)	Yield Stress (MPa)	UTS (MPa)	E <sub>UTS</sub>	Std Dev	Hardness HV
-	-	169.158	189.41	0.1685	0.03	70
1	70	117.44	146.91	0.148	0.0015	83
6	70	134.33	157.24	0.155	0.0210	79
12	70	164.00	190.73	0.154	0.0159	79
24	70	80.12	108.42	0.129	0.0070	65
48	70	165.04	182.38	0.171	0.0070	86
72	70	89.72	99.72	0.154	0.0120	84
1	90	143.87	170.49	0.163	0.0521	84
6	90	146.66	163.60	0.153	0.0152	79
12	90	170.74	189.78	0.165	0.0195	80
24	90	119.95	138.76	0.171	0.0175	69
48	90	142.15	157.66	0.165	0.0255	82
72	90	149.32	163.93	0.157	0.0015	85

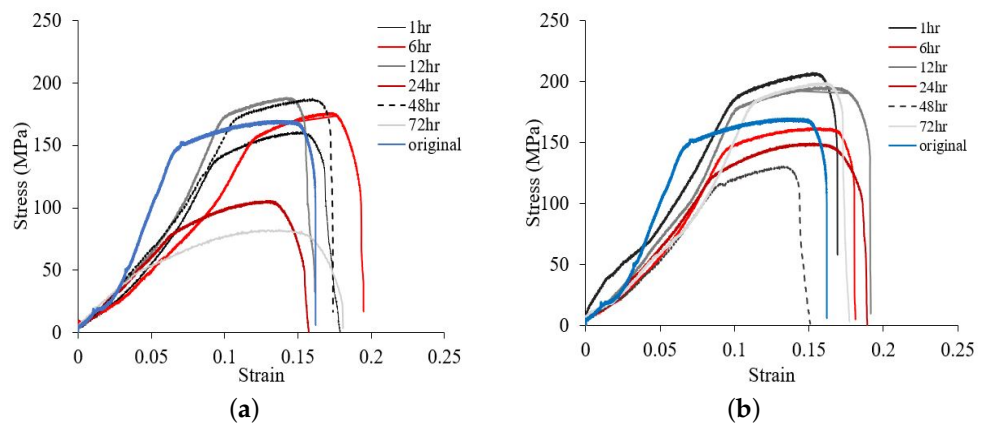


**Figure 3.** Stress strain curves of heat-treated aluminium, in comparison with an original 6063 T5 aluminium. (a) 70 °C and (b) 90 °C.

### 3.2. Finite Element Simulation

To define the position and geometry of the deformation initiators, a finite element simulation was performed. The parameters required for the elastoplastic material were obtained from the tensile stress test and averaged, as summarised in Table 1.

By a convergence study, a mesh size of 2 mm was determined, and a square finite element was selected. Quasi-static compression was performed by inducing displacement of the nodes of the upper side of the tube, and the displacement rate was the same as that of the universal testing machine, 70 mm/min downwards.

A rigid wall on the bottom side of the tube reproduced the boundary condition expressed by the displacement as in the universal testing machine, and the rigid wall was also used as the sensor for crushing force during collapse. A sensor for measuring the energy change during collapse is placed on the tube component (Figure 4). Contact type 7 is established between the elements of the tube and nodes of the mesh to determine if the component is in contact with itself during collapse. This contact is a general-purpose contact between a set of nodes and a master surface, which take into account self-impact, generated by the buckling during the crush process.

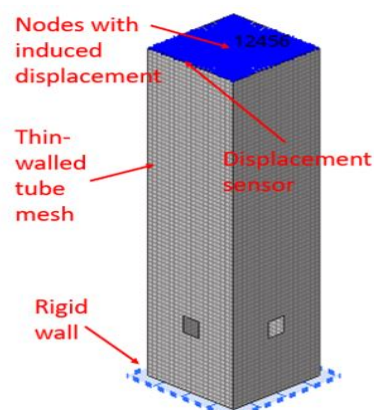


**Figure 4.** Finite element analysis configuration of quasi-static crushing.

The simulation time step is set as  $3.5 \times 10^{-7}$ , which is equal to the node size over the sound speed on aluminium. To determine the energy absorption capacity from the data of the simulation and compare it with the simulation, data are measured every 0.01998 s, which is the same sample rate of the universal testing machine.

### 3.3. Specimen

Specimens are made from a 6063 T5 aluminium square tube with a thickness of 2 mm and 1.5 mm. To determine the mechanical properties of the material, a tensile universal test specimen was made from one side of a tube, and machining process was also performed on a CNC Haas milling machine. In the first experimental phase, 32 specimens were manufactured and tested, and the objective of this experimental phase was to determine the interaction of the trigger area, geometry and location along the major axis of the tube. The location of the trigger mechanism is measured from the upper side of the tube (location where the crusher first touches the tube during collapse) and the geometrical centre of the trigger. Geometrical parameters were evaluated to analyse the geometric effect as a triggering mechanism, as shown in Figure 5. The design variables of the experimental phase are shown in Table 2.

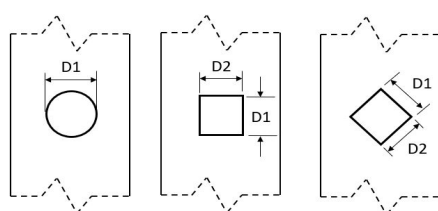


**Figure 5.** Geometrical parameters of trigger, from left to right: circle, square/rectangle and diamond.

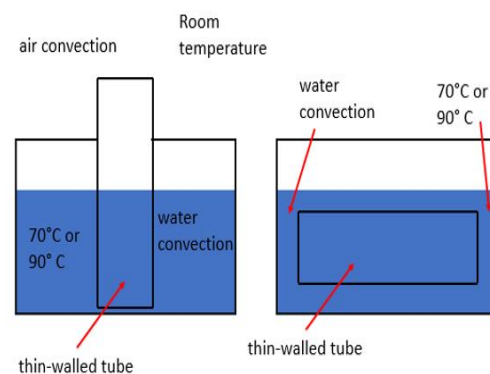
**Table 2.** Experimental design for geometric triggering.

Geometry	Distance from the Upper Side (mm)	D1 (mm)	D2 (mm)
Circle	40, 80, 120, 160	10	
Circle	40, 80, 120, 160	25	
Square	40, 80, 120, 160	10	10
Square	40, 80, 120, 160	25	25
Diamond	40, 80, 120, 160	10	10
Diamond	40, 80, 120, 160	25	25
Rectangle	40, 80, 120, 160	10	15
Rectangle	40, 80, 120, 160	25	37.5

In the heat treatment experimental design, three design variables were selected: furnace time, cooling method temperature and cooling method distribution. For each combination of design variables, two replications were performed, and a total of 24 specimens were made. The combinations of specimens are summarised in Table 3. For all specimens, the furnace temperature was 175 °C. After removal from the furnace, all specimens were cooled for 10 min on the cooling liquid. Cooling rates were for half soaked in water at 70 °C and 90 °C, for 0.43 °C/min and 1.177 °C/min respectively. For the tube completely submerged at 70 °C and 90 °C, the cooling rate is 0.569 °C/min and 1.345 °C/min, respectively. An additional variation was added to the experimental phase, which consisted of inverting the soaking method to a half-soaked method, i.e., the unsoaked part was where the trigger was not implemented, as shown in Figure 6.

**Table 3.** Heat treatment experimental design.

Furnace Time (h)	Cooling Method Temperature (°C)	Soaking Method
1	70, 90	Half soaked, completely soaked
6	70, 90	Half soaked, completely soaked
12	70, 90	Half soaked, completely soaked
24	70, 90	Half soaked, completely soaked
48	70, 90	Half soaked, completely soaked
72	70, 90	Half soaked, completely soaked

**Figure 6.** Half soaked and completely soaked.

#### 4. Results and Discussion

Finite element analysis was configured using Altair *RADIOSS*, and due to low dynamic and inertial effects in quasi-static crushing, it was configured as an implicit simulation. Data collected from the sensor for the crushing force base rigid wall and displacement in the node were used to generate crushing force vs. displacement curves. Each simulated curve was compared with the experimental curve and crushed shape.

Corresponding to the second experimental phase, comparing simulation with experimental results, the averages error in peak crushing forces were 12.64% for circular, 26.27% for square, 14.93% for diamond-shaped and 14.57% for rectangular geometries. Then, the average error in the simulation predictions was 17.10%. For the energy absorbed, the error for circles was 1.15%, 6.81% for squares, 3.84% for diamonds and 10.95% for rectangles. Then, on average, the simulation predicted the energy absorbed with an error of 5.6875%.

For the third experimental phase, a similar comparison was made. The error in the peak crushing force for the original area was 16.69%, 17.99% for 1.5 times the area, 16.65% for 2 times the area and 16.15% for 2.5 times the area. Then, on average, the simulation predicted the peak crushing force with an error of 16.87%. The average error for energy absorbed in the original area was 3.83%, 1.1% for 1.5 times the original area, 7.25% for 2 times the original area and 3.73% for 2.5 times the original area. Then, the simulation predicted the energy absorbed with an error of 3.97%. In Figures 7 and 8, the collapse behaviours of the second and third experiments for the simulation and experiments were compared.

Using the energy efficiency calculated from the simulation data, it was determined that the best geometry was rectangular, and the best size was 2.5 times the original area (250 mm<sup>2</sup>), as is shown in table 4. The same conclusions were obtained using experimental data, showing that even though the data obtained from simulations were not one hundred percent equal to the experimental data, the same tendencies for energy absorbed and peak crushing force were observed among the simulated data, allowing us to reach the same results as the experiments (Figure 9). An area of opportunity within the finite element simulation should be able to represent the properties after the heat treatment, eventually using the generated thermal forces as an initial force field or updating a strain–stress curve

to represent the properties of the component. However, it is not possible to reproduce the entire cooling process and generate complex numerical models to reproduce the entire generated process, and because of this, physical tests are considered essential.

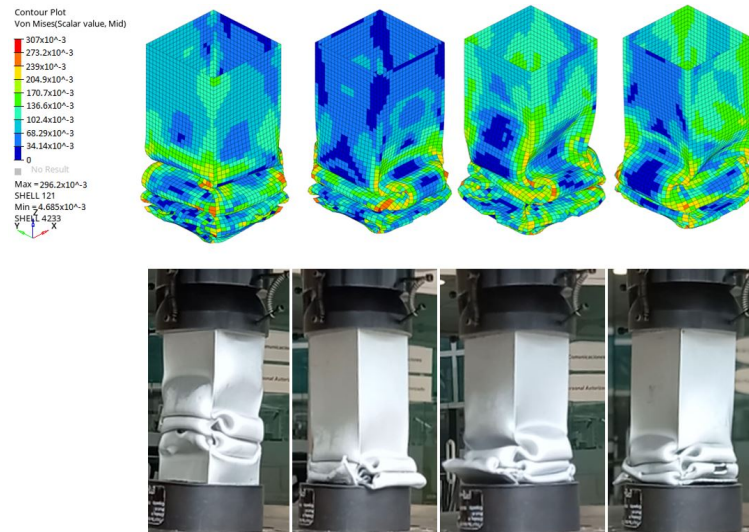


**Figure 7.** Collapse behaviour of the same area and distance from the upper side, from left to right: circular, square, diamond-shaped and rectangular geometries. Comparison of simulations with experimental data, 85.714 s.

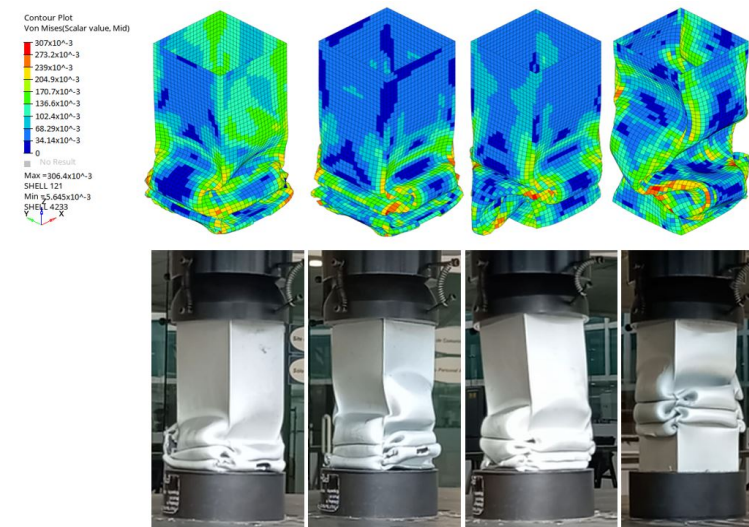


**Figure 8.** Collapse behaviour of the same geometry and distance from the upper side, from left to right: 1, 1.5 times, 2 times and 2.5 times the original area. Comparison of simulations with experimental data, 85.714 s.

**Table 4.** Energy efficiency from the simulation for the second and third experimental phase.

	Energy Efficiency		Energy Efficiency
circle	0.206	original area	0.224
square	0.208	1.5 original area	0.237
diamond	0.219	2 original area	0.220
rectangle	0.224	2.5 original area	0.251

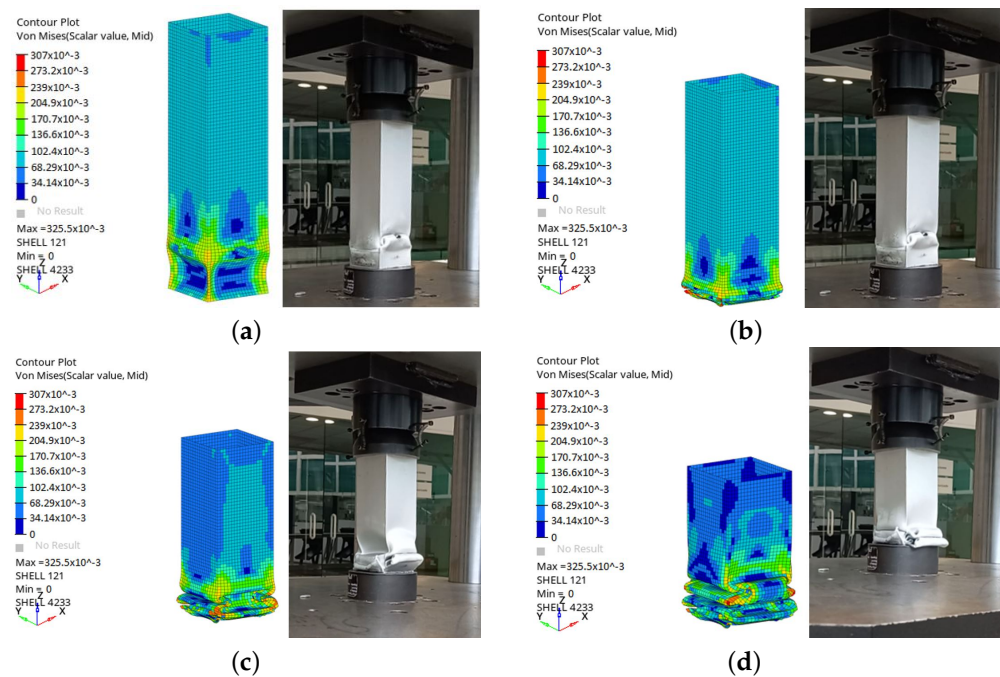


**Figure 9.** Evolution of the collapse simulation and experiment: (a) 7 s, (b) 32 s, (c) 57 s and (d) 86 s.

The purpose of adding triggering mechanisms to thin-walled tubes is to prevent global buckling and favour localised buckling, which leads to progressive buckling. When the tube collapses in a progressive way, energy absorption increases due to longer deformation distances by formation of plastic folds. Depending on tube stiffness, material ductility and geometrical imperfections, three possible deformation modes during collapse were observed. In Figure 10a, the first plastic fold formed around the trigger, but the remaining material was not strong enough to form a subsequent plastic fold. As the crushing continued, the tube broke near the deformed area, fracture propagated, and no folding continued. In Figure 10b, plastic folds formed near the base. Folds formed successfully, but near the base, deformation formed around the fold, leading to a fracture. Instead of forming a new plastic fold, the first formed kept deforming until it broke. In Figure 10c, the fold formed successfully and symmetrically. Therefore, a new plastic fold formed near the first fold, and subsequent plastic folds formed until the tube completely collapsed.

Figure 11 shows the relationship of the load vs. displacement curve and the deformation of the thin-walled tube. In Figure 11a, the peak crushing force was reached as soon as the crusher started applying force on the tube and before any deformation was appreciable. In Figure 11b, the tube strength decreased due to deformation, so a reduction in crushing force was seen. In Figure 11c, plastic deformation increased, leading to a sudden increase in strength due to strain hardening, and plastic folds began to form. In Figure 11d, a new plastic fold formed close to the previous fold, and the crushing force decreased. In Figure 11e, the crushing force increased because the formed plastic fold compressed over itself, and when new plastic folds started to form, the load decreased again. The process repeated until all the plastic folds formed and the tube completely collapsed.

In Figure 12, examples of specimens of each experimental phase are shown. In Figure 12a, even though a first plastic fold formed, if the trigger was located near the upper corner, then shearing instead of formation of a second fold was more common. The probability of formation of subsequent plastic folds after the first increased with increasing distance from the upper side. Figure 12b shows that the rectangular trigger allowed more symmetric folds to form, resulting in more stable collapse. In Figure 12c, 2.5 times the trigger area increased the number of plastic folds formed before shearing, increasing the energy absorbed. Finally, in Figure 12d, the cooling method changed the folding behaviour, resulting in different energy absorption indicator values. This finding is consistent with that of

Nikkhah et al. (2023) [35], who concluded that the forming history has an effect on the energy absorption performance.

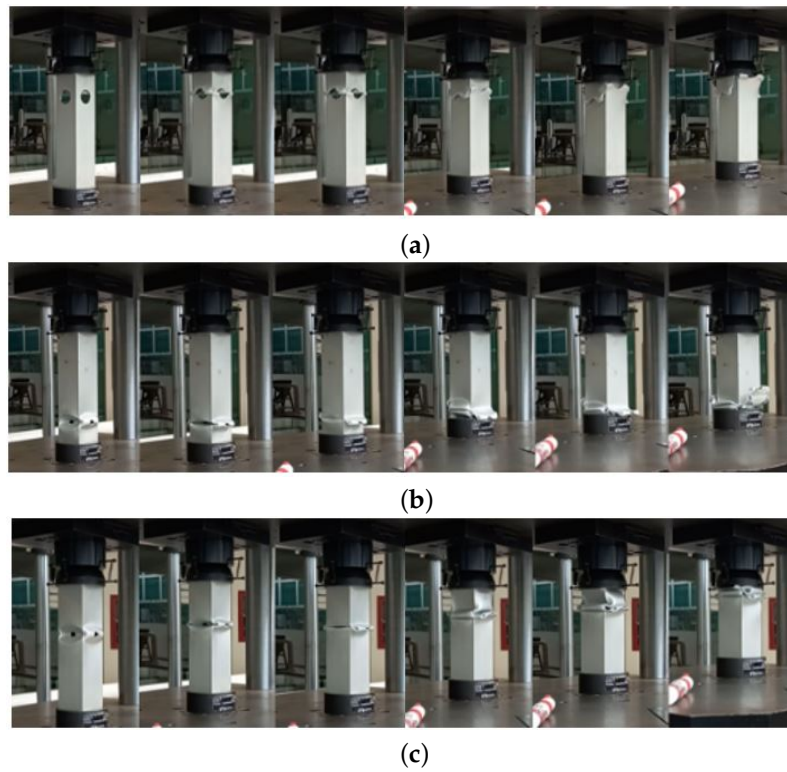


Figure 10. Collapse mode. (a) Big trigger mechanism geometry, (b) with shearing and (c) without shearing.

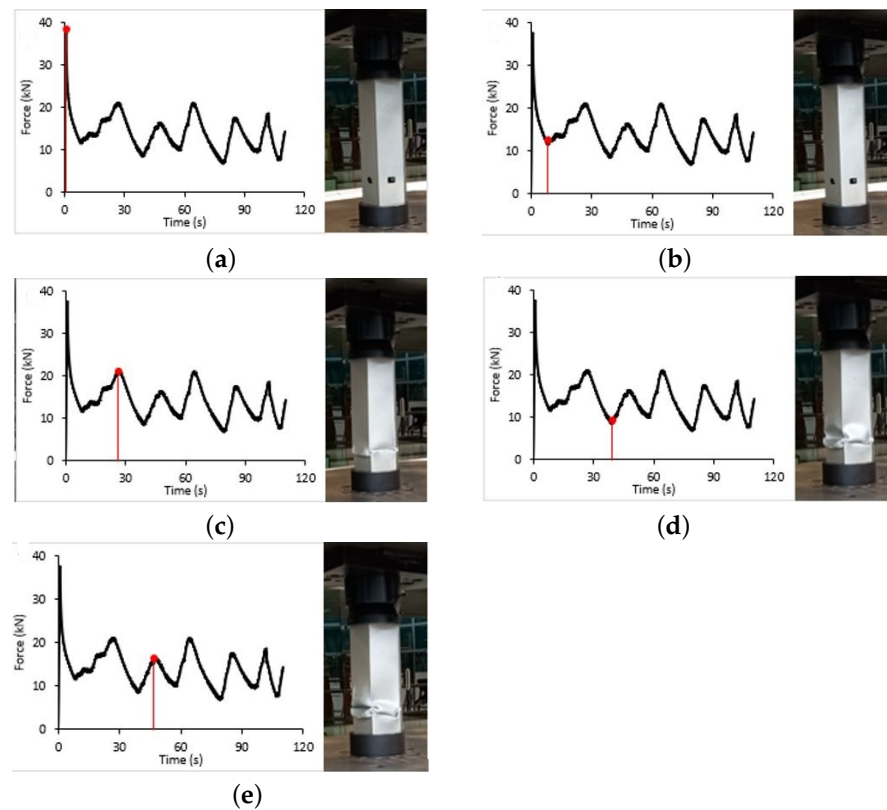
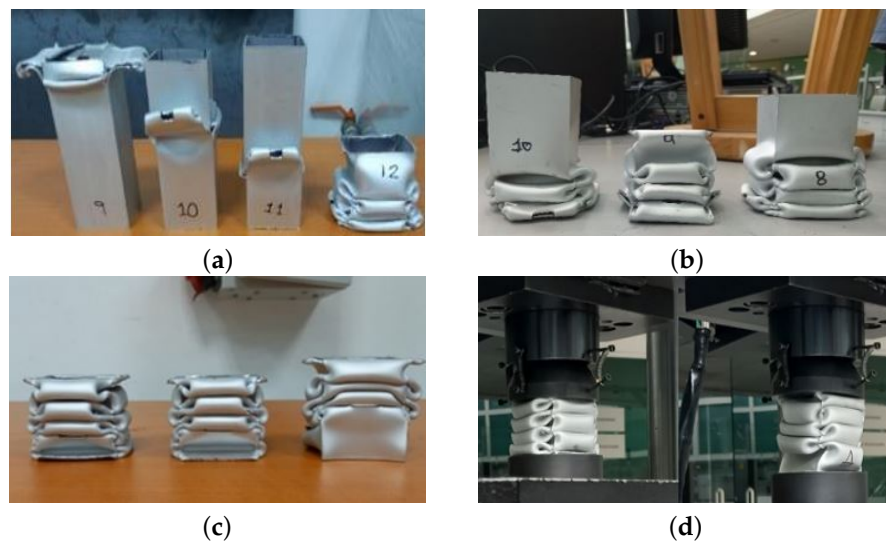
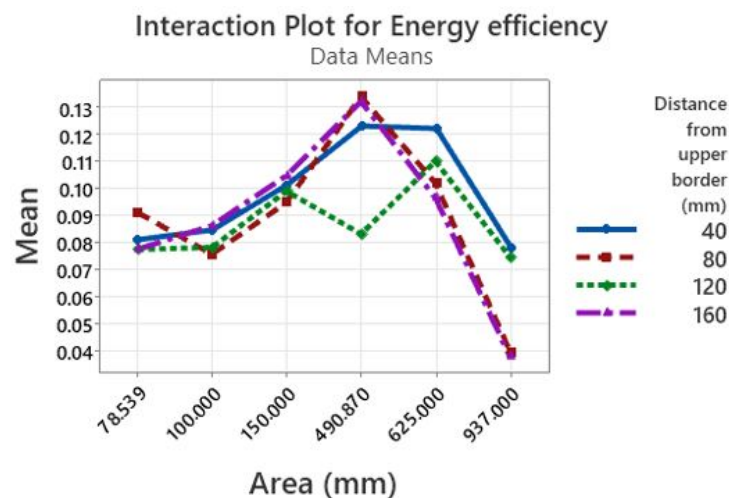


Figure 11. Relation of crushing force vs displacement curve with deformation of tube during collapse, (a) highest peak force, (b) start of first fold, (c) triggers collapse, (d) start of second fold and (e) collapse propagation.



**Figure 12.** Different collapse responses. (a) Deformed tube for rectangle/100 mm<sup>2</sup> from 40 mm to 160 mm from the upper side, (b) rectangle/99.96 mm<sup>2</sup>/160 mm from the upper side, (c) rectangle/249.99 mm<sup>2</sup>/160 mm from upper side, and (d) 175 °C/72 h/70 °C complete and 175 °C/72 h/70 °C half cooled.

Crushing force vs. displacement data obtained from the experimental test were used to calculate the energy absorption indicator and then compared to the tube without modification to determine the design performance. It was observed from the experimental test that for small areas of trigger, progressive buckling was more likely. If the trigger was closer to the base, then it was more probable that the tube collapsed progressively instead of fracturing after the first fold. A larger trigger area drastically reduced the peak crushing force but also increased the probability of fracture and incomplete fold formation. The peak crushing force decreased as the trigger area increased. Until 150 mm<sup>2</sup> of trigger area, the energy absorbed increased with increasing area, after which it drastically decreased with increasing area. The energy efficiency increased until 490.7 mm<sup>2</sup> trigger area, after which it decreased with increasing trigger area. Alone, the distance from the upper side did not have an effect on the crushing force, energy absorbed and energy efficiency, but considering its interaction effect with the trigger area, the best combination of both parameters was from 100 mm<sup>2</sup> to 490.87 mm<sup>2</sup> area and 160 mm distance from the upper side, with the greatest energy efficiency. The best distance from the upper side, under this range of trigger area, was 160 mm. The interaction effects of the design variables are shown in Figure 13.



**Figure 13.** Interaction of design variables over energy efficiency for the first experimental phase.

The trigger area and distance from the upper side were fixed to 100 mm<sup>2</sup> and 160 mm, respectively. The rectangle had the smallest peak crushing force, and the square geometry had the largest. The rectangle has the largest energy absorbed, while the square had the smallest. From largest to smallest crushing force efficiency, the results were: diamond, circle, rectangle, square. The diamond design had the greatest crushing force efficiency, but with only 2.89% difference from the rectangular design. Taking energy efficiency as the determining parameter, the rectangle had the greatest value. Then, from this experimental design, it was determined that the rectangular geometry had the best energy absorption characteristics. A comparison of the energy absorption indicators of the design variable levels and unmodified levels is shown in Figure 14.

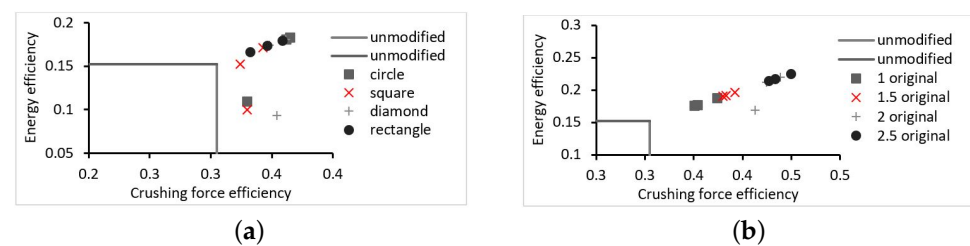


**Figure 14.** Energy absorption indicators for specimens for second experimental phase, (a) effect of the shape of the initiator and (b) effect of the effective area of the collapse.

To determine the optimal trigger area, the distance from the upper side and geometry was fixed to rectangular, obtained from the previous experimental phase, and 160 mm from the upper side. The absorbed energy increased from 1 to 1.5, then decreased from 1.5 to 2 and increased again from 2 to 2.5. The crushing force efficiency increased with the trigger area due to the lower peak crushing force and more stable collapse. Energy efficiency increased with increasing trigger area. Considering all four curves, the trigger area with better crashworthiness characteristics was 2.5 times the original area. A comparison of the energy absorption indicators of the design variable levels and unmodified levels is shown in Figure 15.

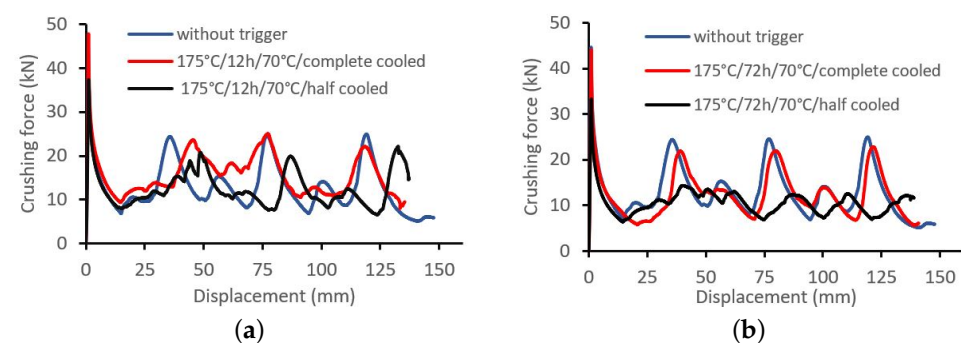


**Figure 15.** Crushing force vs. displacement curve for different cooling methods: (a) 24 h and (b) 72 h in the furnace.

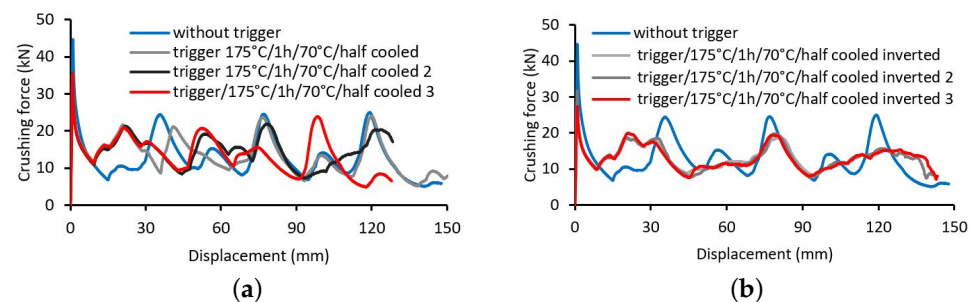
The design variables were the time in the furnace, the temperature of the cooling liquid (water) and whether the entire specimen or only half of its length was soaked, leaving the unsoaked part to be cooled by room temperature air. The specimen remained in water for 10 min and then was placed on a table until it was tested. The part that was half cooled developed a varying strength region due to different cooling rates between the soaked base and the unsoaked tip. Half-cooled tubes presented a greater reduction in peak crushing force compared to completely cooled tubes, as shown in Figure 15a. The subsequent crushing force peaks of completely cooled tubes after the first peak remained the same as those of tubes without treatment, while the half-cooled peak is drastically reduced.

Figure 15b shows that heat treatment could reduce crushing force peaks to approximately a straight line, and at the same time decreasing the peak deceleration during crushing.

The peak crushing force decreased with increasing time in the furnace and increased with higher cooling temperature and total sucking. From 1 to 12 h, the energy absorbed decreased with the furnace time, and after 12 h, it increased but at a lower rate. Lower cooler temperature and total cooling increased energy absorption. The mean crushing force had the same behaviour as the peak crushing force, showing that the reduction in force was, in most cases, equal for the peak crushing force and subsequent peaks. Energy efficiency decreased from 1 to 6 h in the furnace, remained the same from 6 to 12 h, increased sharply from 12 to 48 h and decreased again from 48 to 72 h. A lower cooler temperature increased the energy efficiency due to smaller yield strength caused by a combination of number and size of precipitated phases, which resulted in a smaller peak crushing force.

Combinations of 70 °C and half soaked samples had the greatest energy efficiency. The optimal heat treatment configuration was in the furnace at 175 °C for 1 h and cooled in water at 70 °C only soaking half of the length.

The selected trigger geometry and heat treatment method from the previous experimental phase were implemented using the same thin-walled tube and then tested experimentally to determine the energy absorption indicators. A comparison was made between the proposed designs and a tube with only a trigger and a tube with only heat treatment. In Figure 16a,b a comparison with a tube without a trigger and treatment is performed to determine whether the combined method was better than each separate method.



**Figure 16.** Crushing force vs. displacement curves for (a) thin-walled tube with trigger and heat treatments and (b) thin-walled tube with trigger and inverted heat treatment.

On average, triggering at 175 °C/1 h/70 °C/half cooled reduced the peak crushing force by 21.63% and increased the energy absorption by 42.53%, resulting in an increase in the energy efficiency of 81.9% in comparison with the thin-walled tube without the mechanism implemented. The inverted cooling method on average reduced the peak crushing force by 33.92% and increased energy absorption by 40.33%, resulting in a 97.07% increase in energy efficiency.

Both methods effectively reduced the peak crushing force and increased energy absorption in comparison with thin-walled tubes without a mechanism implemented rather than heat treatment and trigger alone. The inverted method enhanced energy absorption indicators in a greater way than the normal method, but collapse was more stable with the conventional method.

A comparison with 6063 T5 without treatment is shown in Figure 17. The furnace time increased the yield stress, which increased the mechanical strength of the tube, and cooling at 90 °C increased the yield strength. More furnace time allowed the dissolution of more precipitated phase from the previous heat treatment, resulting in a more homogenous phase. Slower cooling reduced the growth of the precipitated phase, leaving small and numerous strong phases on a soft matrix. The comparison of mechanical properties and energy absorption indicators showed that energy efficiency was inversely proportional to yield stress under certain intervals, which was due to the reduction in peak crushing force but the increase in ductility, which increased the area under the curve.

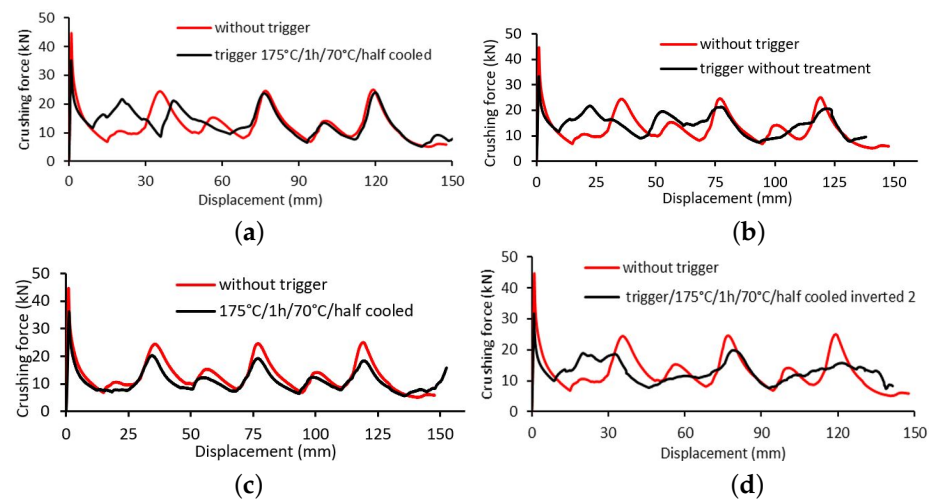


**Figure 17.** Comparison of crushing force vs. displacement curves. (a) Tubes without the enhancement mechanism and triggers without treatment, (b) a tube without modifications and a treated tube without triggers, (c) a tube without modifications and a tube with triggers and heat treatment, and (d) a tube without modification and a tube with both triggers and heat treatment.

Hardness increased with increasing yield strength, only showing an increased from 80 to 83 HV, and then continued linear behaviour. Comparing hardness with metallography obtained from heat-treated aluminium, the smaller hardness value was related to the low concentration of the precipitated phase (darker dots) in Figure 18, except for 48 h/90 °C and 48 h/70 °C. Generally, for the same time in a furnace, cooling in warmer water increased hardness and yield strength.

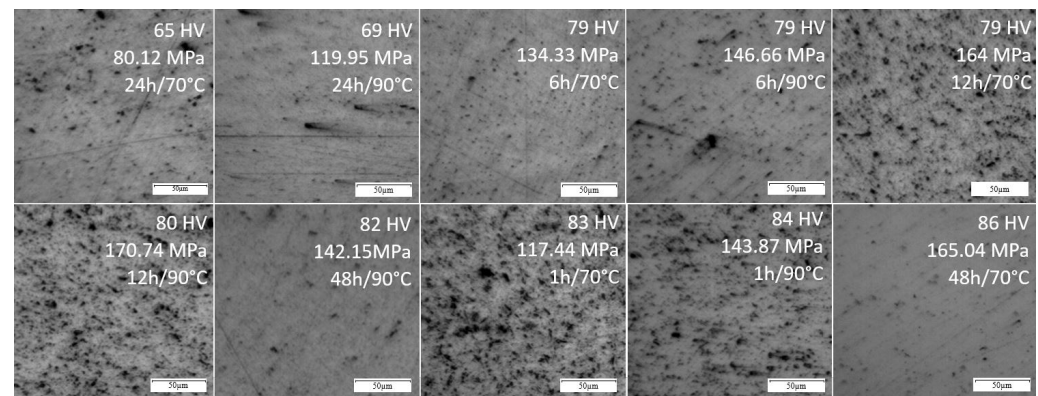


**Figure 18.** Metallography of heat treatment combinations in an optical microscope.

Mechanical discontinuities improves the crashworthiness performance of aluminium, and can be used to control the energy absorption evolution [22,36]. Most striking was the substantial difference in energy absorbed among the components. Figure 19 shows the comparison between the components as delivered, with trigger but without treatment and with trigger and treatment. It is observed that the three components have a similar tendency up to 15 mm of displacement; however, in the maximum deformation, the lowest energy is achieved with the component as delivered, and although the element with the highest energy absorbed is only with the thermal treatment, the component with thermal treatment and trigger is the one that best controls the force and deceleration peaks throughout the deformation.

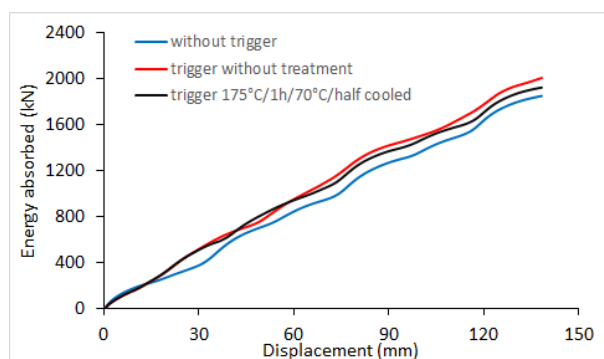


**Figure 19.** Energy absorbed vs. displacement.

## 5. Conclusions

This study set out to enhance the crashworthiness enhancement methods to obtain the optimal peak crushing force and energy absorption for design applications. It was a consequence of the employment of thin-walled structures, which are commonly used for lightweight applications owing to their high strength and light mass. In this work, aluminium was used as the material due to high ductility and strength-to-weight ratios, which are even greater than those of steel. This study has identified that without any modification, thin-walled tubes with a configuration of side size, thickness and length deform progressively, forming plastic folds until the structure completely deformed. This deformation mode allows structures to absorb great quantities of energy.

The results of this investigation also show that it is possible to improve crashworthiness enhancement methods by combining methods such as trigger mechanisms and heat treatments. The heat treatment was used to artificially accelerate the deterioration of tubes, which can also increase energy absorption and reduce peak crushing force. Therefore, the best configuration from both techniques is implemented using the same tube. This implementation gave a reduction of 21.63% of peak crushing force and an increase of 42.53% on energy absorbed, compared with a tube without modifications. In other words, an 81.90% enhancement of energy efficiency was obtained by implementing both methods. The contribution of this study has been to confirm that the proposed crashworthiness enhancement method can reduce the peak crushing force and increase the energy-absorption capacity of the components.

**Author Contributions:** Conceptualisation, M.J.-M. and J.J.-A.; methodology, M.J.-M. and J.V.-S.; validation, J.J.-A., J.V.-S. and M.J.-M.; formal analysis, J.J.-A., J.V.-S. and M.J.-M.; investigation, J.J.-A., J.V.-S. and M.J.-M.; resources, M.J.-M.; data curation, J.J.-A. and J.V.-S.; writing—original draft preparation, J.J.-A., J.V.-S., A.S.D., R.P.S. and M.J.-M.; writing—review and editing, M.J.-M.; visualisation, J.J.-A., J.V.-S. and M.J.-M.; supervision, M.J.-M. All authors have read and agreed to the published version of the manuscript.

**Funding:** This research received no external funding.

**Data Availability Statement:** The data presented in this study are available on request from the corresponding author.

**Conflicts of Interest:** The authors declare no conflict of interest.

## References

- Jimenez-Martinez, M. Artificial Neural Networks for Passive Safety Assessment. *Eng. Lett.* **2022**, *30*, 289–297.
- Wang, X.; Sun, P.; Zuo, W.; Bai, J. Multi-objective optimization of automobile body frame considering weight, rigidity, and frequency for conceptual design. *Adv. Mech. Eng.* **2022**, *14*, 16878132221078495. [[CrossRef](#)]
- Arora, S.; Kapoor, A. Mechanical Design and Packaging of Battery Packs for Electric Vehicles. In *Behaviour of Lithium-Ion Batteries in Electric Vehicles: Battery Health, Performance, Safety, and Cost*; Pistoia, G., Liaw, B., Eds.; Springer International Publishing: Cham, Switzerland, 2018; pp. 175–200.
- Patel, V.; Tiwari, G.; Dumpala, R. Review of the crushing response of collapsible tubular structures. *Front. Mech. Eng.* **2020**, *15*, 438–474. [[CrossRef](#)]

5. Dima, D.S.; Covaciu, D. Vehicles Frontal Impact Analysis Using Computer Simulation and Crash Test. *Int. J. Automot. Technol.* **2019**, *20*, 655–661. [[CrossRef](#)]
6. Anselma, P.G.; Niuotta, C.; Mainini, L.B.; Belingardi, G. Multidisciplinary design optimization for hybrid electric vehicles: Component sizing and multi-fidelity frontal crashworthiness. *Struct. Multidiscip. Optim.* **2020**, *62*, 2149–2166. [[CrossRef](#)]
7. Yu, L.; Gu, X.; Qian, L.; Jiang, P.; Wang, W.; Yu, M. Application of tailor rolled blanks in optimum design of pure electric vehicle crashworthiness and lightweight. *Thin-Walled Struct.* **2021**, *161*, 107410. [[CrossRef](#)]
8. Hou, W.; He, P.; Yang, Y.; Sang, L. Crashworthiness optimization of crash box with 3D-printed lattice structures. *Int. J. Mech. Sci.* **2023**, *247*, 108198. [[CrossRef](#)]
9. Wang, G.; Zhang, Y.; Zheng, Z.; Chen, H.; Yu, J. Crashworthiness design and impact tests of aluminum foam-filled crash boxes. *Thin-Walled Struct.* **2022**, *180*, 109937. [[CrossRef](#)]
10. Sun, G.; Tian, J.; Liu, T.; Yan, X.; Huang, X. Crashworthiness optimization of automotive parts with tailor rolled blank. *Eng. Struct.* **2018**, *169*, 201–215. [[CrossRef](#)]
11. Prasetya, L.W.; Prabowo, A.R.; Ubaidillah, U.; Istanto, I.; Nordin, N.A.B. Design of crashworthy attenuator structures as a part of vehicle safety against impact: Application of waste aluminum can-based material. *Theor. Appl. Mech. Lett.* **2021**, *11*, 100235. [[CrossRef](#)]
12. Baroutaji, A.; Arjunan, A.; Niknejad, A.; Tran, T.; Olabi, A.G. Application of Cellular Material in Crashworthiness Applications: An Overview. In *Reference Module in Materials Science and Materials Engineering*; Elsevier: Glasgow, Scotland, 2019.
13. Lu, R.; Gao, W.; Hu, X.; Liu, W.; Li, Y.; Liu, X. Crushing analysis and crashworthiness optimization of tailor rolled tubes with variation of thickness and material properties. *Int. J. Mech. Sci.* **2018**, *136*, 67–84. [[CrossRef](#)]
14. Sun, G.; Chen, D.; Zhu, G.; Li, Q. Lightweight hybrid materials and structures for energy absorption: A state-of-the-art review and outlook. *Thin-Walled Struct.* **2022**, *172*, 108760. [[CrossRef](#)]
15. Vignjevic, R.; Liang, C.; Hughes, K.; Brown, J.C.; De Vuyst, T.; Djordjevic, N.; Campbell, J. A numerical study on the influence of internal corrugated reinforcements on the biaxial bending collapse of thin-walled beams. *Thin-Walled Struct.* **2019**, *144*, 106277. [[CrossRef](#)]
16. Jiang, B.; Chen, X.; Yu, J.; Zhao, Y.; Xie, Z.; Tan, H. Energy-absorbing properties of thin-walled square tubes filled with hollow spheres. *Thin-Walled Struct.* **2022**, *180*, 109765. [[CrossRef](#)]
17. Song, J.; Xu, S.; Xu, L.; Zhou, J.; Zou, M. Experimental study on the crashworthiness of bio-inspired aluminum foam-filled tubes under axial compression loading. *Thin-Walled Struct.* **2020**, *155*, 106937. [[CrossRef](#)]
18. Tak, S.; Iqbal, M. Axial compression behaviour of thin-walled metallic tubes under quasi-static and dynamic loading. *Thin-Walled Struct.* **2021**, *159*, 107261. [[CrossRef](#)]
19. Baaskaran, N.; Ponappa, K.; Shankar, S. Quasi-Static Crushing and Energy Absorption Characteristics of Thin-Walled Cylinders with Geometric Discontinuities of Various Aspect Ratios. *Lat. Am. J. Solids Struct.* **2017**, *14*, 1767–1787. [[CrossRef](#)]
20. Alshahrani, H.; Sebaey, T.A.; Allah, M.M.A.; El-baky, M.A.A. Quasi-static axial crushing performance of thin-walled tubes with circular hole discontinuities. *J. Compos. Mater.* **2022**, *56*, 4195–4218. [[CrossRef](#)]
21. Montazeri, S.; Elyasi, M.; Moradpour, A. Investigating the energy absorption, SEA and crushing performance of holed and grooved thin-walled tubes under axial loading with different materials. *Thin-Walled Struct.* **2018**, *131*, 646–653. [[CrossRef](#)]
22. Estrada, Q.; Szwedowicz, D.; Silva-Aceves, J.; Majewski, T.; Vergara-Vazquez, J.; Rodriguez-Mendez, A. Crashworthiness behavior of aluminum profiles with holes considering damage criteria and damage evolution. *Int. J. Mech. Sci.* **2017**, *131–132*, 776–791. [[CrossRef](#)]
23. Kathiresan, M. Influence of shape, size and location of cutouts on crashworthiness performance of aluminium conical frusta under quasi-static axial compression. *Thin-Walled Struct.* **2020**, *154*, 106793. [[CrossRef](#)]
24. Westermann, I.; Pedersen, K.; Børvik, T.; Hopperstad, O. Work-hardening and ductility of artificially aged AA6060 aluminium alloy. *Mech. Mater.* **2016**, *97*, 100–117. [[CrossRef](#)]
25. Baganis, A.; Bouzouni, M.; Papaefthymiou, S. Phase Field Simulation of AA6XXX Aluminium Alloys Heat Treatment. *Metals* **2021**, *11*, 241. [[CrossRef](#)]
26. Karantza, K.D.; Manolakos, D.E. Crashworthiness Analysis of Square Aluminum Tubes Subjected to Oblique Impact: Experimental and Numerical Study on the Initial Contact Effect. *Metals* **2022**, *12*, 1862. [[CrossRef](#)]
27. Acar, E.; Altin, M.; Güler, M. Evaluation of various multi-cell design concepts for crashworthiness design of thin-walled aluminum tubes. *Thin-Walled Struct.* **2019**, *142*, 227–235. [[CrossRef](#)]
28. Tao, Y.; Wang, Y.; He, Q.; Xu, D.; Li, L. Comparative Study and Multi-Objective Crashworthiness Optimization Design of Foam and Honeycomb-Filled Novel Aluminum Thin-Walled Tubes. *Metals* **2022**, *12*, 2163. [[CrossRef](#)]
29. Zhang, J.; Zheng, D.; Lu, B.; Liu, Q. A numerical and theoretical study on crushing behaviours of variable thickness 12 right-angles section tubes. *Int. J. Crashworthiness* **2022**, *27*, 168–180. [[CrossRef](#)]
30. Christensen, J.; Wilson, A.; Bastien, C.; Kayvantash, K. Efficient crash structure design for road traffic accidents of tomorrow. *Int. J. Crashworthiness* **2022**, 1–20. [[CrossRef](#)]
31. Li, Y.; Fan, Z.; Hu, S.; Zhang, F.; Hu, L.; Xue, Z. Mechanical performance of multi-cell thin-walled tubes under static and dynamic axial loading. *Int. J. Crashworthiness* **2023**, 1–11. [[CrossRef](#)]
32. Yalçın, M.M.; Genel, K. Crashworthiness performance of novel pre-deformation method applied square aluminum tubes. *Int. J. Crashworthiness* **2022**, 1–12. [[CrossRef](#)]

33. Teixeira, P.; Pina, L.; Rocha, R.; Sadek, S. Parametric analysis of energy absorption capacity of thin aluminum plates impacted by rigid spherical projectiles. *Thin-Walled Struct.* **2021**, *159*, 107240. [[CrossRef](#)]
34. Dubey, R.; Jayaganthan, R.; Ruan, D.; Gupta, N.; Jones, N.; Velmurugan, R. Energy absorption and dynamic behaviour of 6xxx series aluminium alloys: A review. *Int. J. Impact Eng.* **2023**, *172*, 104397. [[CrossRef](#)]
35. Nikkhah, H.; Naveed, N.; Beiragh, R.A.; Dadashzadeh, S.; Truong, Q.T. Crashworthiness investigation of draw bead in aluminum tubes under axial loading condition. *Int. J. Prot. Struct.* **2023**, *14*, 107–121. [[CrossRef](#)]
36. Zang, M.; Hu, Y.; Zhang, J.; Ye, W.; Zhao, M. Crashworthiness of CFRP/aluminum alloy hybrid tubes under quasi-static axial crushing. *J. Mater. Res. Technol.* **2020**, *9*, 7740–7753. [[CrossRef](#)]

**Disclaimer/Publisher's Note:** The statements, opinions and data contained in all publications are solely those of the individual author(s) and contributor(s) and not of MDPI and/or the editor(s). MDPI and/or the editor(s) disclaim responsibility for any injury to people or property resulting from any ideas, methods, instructions or products referred to in the content.